Journal of Innovative Technology, Vol. 4, No. 1, pp. 13-21, March 2022
http://doi.org/10.29424/JIT.202203_4(1).0003

Design and Hardware Implementation of a Variable Speed Wind Turbine Emulator System

Chao-Tsung Ma [1*] and Yu-Hung Ho [2]

ABSTRACT

Wind turbine power generation has become increasingly prevalent in recent years, and the related research topics continue to generate deep research interest. In order to further improve the research efficiency and provide convenience in conducting wind energy conversion system (WECS) research, this paper aims to design and implement a hardware emulation system for the variable speed permanent magnet synchronous wind turbine generator (WTG). The proposed WTG emulator system includes (1) a wind turbine emulator (WTE) unit composed of a three-phase permanent magnet synchronous motor (PMSM) and a torque controller and (2) a three-phase permanent magnet synchronous generator (PMSG). In order to verify the correctness and feasibility of the proposed WTE system, the power control interface for the PMSG adopts a simple three-phase full-bridge rectifier and a boost converter to facilitate maximum power point tracking (MPPT) control for various WTE functional tests. The main focuses of this paper include mathematical model derivation and simulation of WTE as well as the design and implementation of three-phase PMSM torque tracking controllers, i.e., proportional (P), proportional integral (PI), and fuzzy controllers, respectively. Typical simulation and implementation results are presented to verify the feasibility and effectiveness of the proposed WTE system.

Keywords: wind turbine emulator (WTE); wind energy conversion system (WECS); permanent magnet synchronous motor (PMSM); permanent magnet synchronous generator (PMSG)

1. INTRODUCTION

Over the past decade, the global economy has grown rapidly, which has raised the demand for electric power. In addition, environmental protection is becoming more and more popular, making the development of traditionally used fossil fuels somewhat difficult. Therefore, the rapid development and commercialization of renewable energy (RE) based power generation has become an inevitable trend. Presently, solar and wind power generation has matured and are widely used in actual commercial conditions. Meanwhile, the capacity of wind energy conversion system (WECS) continues to grow worldwide. This has called for new research on the WECS related themes. In more recent years, due to the significant reduction in the price of power electronics and the advancement of digital control technology, the existing small- and medium-size wind turbine generators (WTGs) on the market mostly adopt PMSG with built-in power electronic controllers. Since the PMSG has no gearbox loss, it has relatively high reliability, high efficiency, and better performance. In addition, because no external DC excitation power supply is required, a complicated control mechanism is not required (Qais, Hasanien & Alghuwainem, 2017). The variable voltage due to wind speed fluctuation can be properly regulated to supply the load through a constant-voltage, constant-frequency power supply interface using power converters.

In practice, the condition of natural wind speed cannot be completely predicted. In order to improve the efficiency and convenience in conducting WECS research, this paper aims to design and practically build a 0.7 kW hardware wind turbine emulation system of the variable speed permanent magnet synchronous WT to facilitate various WECS researches in a laboratory environment. The WTE is composed of a PMSM and a torque controller, which is controlled using P, PI, and Fuzzy controllers (Chen, Li & Chen, 2016; Liu, Hou & Hua, 2019; Shukla & Singh, 2019), respectively. In order to verify the correctness of the proposed WTE system, this paper uses the perturb and observes the MPPT algorithm (Sampaio et al., 2019) for testing the constructed hardware system.

In the open literature, a number of WTE systems can be found. Typical ones are briefly reviewed in the section. Bhayo et al. (2017) have designed a DC motor-DC generator based WTE controlled with two PI controllers. Ajewole et al. (2017) present a DC motor-wound rotor induction generator based WTE. Narayana et al. (2017) study the use of a time series adaptive linear prediction (ALP) technique to improve the dynamic performance of a WECS. The method is tested on a DC shunt motor-PMSG based WTE. Arévalo et al. (2017) have implemented an induction motor-DC generator based WTE with field weakening control technique. Gan, Shek, and Mueller (2017) discuss downhill tower shadow effects using an induction motor-induction generator based WTE connected to a grid emulator. Comprehensive results on simulation and experimental tests were presented. Mohammadi, Fadaeinedjad, and Naji (2018) discuss tower shadow and yaw error effects with experiments on an

Manuscript received February 24, 2021; accepted March 11, 2022.
[1*] Professor (corresponding author), Dept. of EE, CEECS,National United University, Taiwan. (email: ctma@nuu.edu.tw)
[2] Postgraduate Student, Dept. EE, CEECS,National United University, Taiwan.

induction motor-induction generator based WTE. Both AeroDyn and FAST software tools are used to model related aerodynamic and mechanical characteristics. The same WTE is later used (Mohammadi et al., 2018) to analyze horizontal and vertical wind shear effects. Karabacak et al. (2018) have built an induction motor-PMSG based WTE for the study of power converter interfaces in WECSs. Tian et al. (2018) have built an induction motor-PMSG based WTE experimental platform and a "direct decoupling double second-order generalized integral phase-locked loop (DDSOGI-PLL)" was proposed. Guerrero et al. (2017) proposed a torque estimator to provide over torque/current protection for existing soft-stall methods. The method was tested on a squirrel cage induction motor-PMGS based WTE. Merabet et al. (2016) proposed a laboratory-scale microgrid with multiple RE sources, where a permanent-magnet dc motor (PMDCM)-PMSG based WTE. Abdallah et al. (2018) have implemented a PI-controlled WTE based on PMSM-PMSG. Field oriented control was adopted by the authors in the proposed control scheme. Chen et al. (2017) proposed a surface-mounted PMSM-interior PMSG based WTE using heuristically tuned PI controllers.

It is found that most control methods and verification schemes for WTE reported in the above-reviewed papers are too complex to construct easily. This paper attempts to present a simple means for constructing a small-scale TWE for laboratory purposes. This paper is planned as follows: section 2 explains the derivation of a mathematical model of a WT system and uses PSIM to verify the designed WT model. Section 3 explains the derivation of the mathematical model of a PMSG and presents the results of simulation and analysis. Section 4 describes the simulation of a variable-speed permanent magnet synchronous WECS model, the proposed WECS emulator architecture, and the proposed torque controllers used in this paper, and demonstrates the WTE system via typical simulation and implementation results. Section 5 summarizes the findings and tasks completed in this paper.

2. DESIGN AND SIMULATION OF A WT SYSTEM

According to Betz's law, the maximum efficiency of a wind energy-mechanical energy conversion system is about 59.3%. However, in practical applications, the conversion efficiency of most WTs is about 30% to 50%. If one considers the efficiency of electromechanical equipment such as generators, the total output efficiency is further reduced to about 20% to 45%. Coefficient of power $C_p(\lambda,\theta)$ can be used to describe the conversion efficiency of a WT for wind energy-mechanical energy conversion, which is related to the blade pitch angle θ and tip-speed ratio λ. In literature, the blade pitch angle is mostly set to 3° to 5°. In order to capture the maximum wind energy, this study adopts the blade pitch angle of 3°.

Fig. 1(a) shows the C_p-λ characteristic curves for different blade pitch angles [19,20], where λ is related to the blade radius R, angular velocity ω and wind speed U, as shown in (1). To obtain the theoretical maximum value of C_p, θ should be set to 0°, and the optimum value of λ can be calculated as (1). Fig. 1 (b) shows the characteristic curves of mechanical power P_m versus rotational speed N under different wind speeds. It can be seen that there is a unique maximum power point at each wind speed.

$$\lambda = \frac{R\omega}{U}. \tag{1}$$

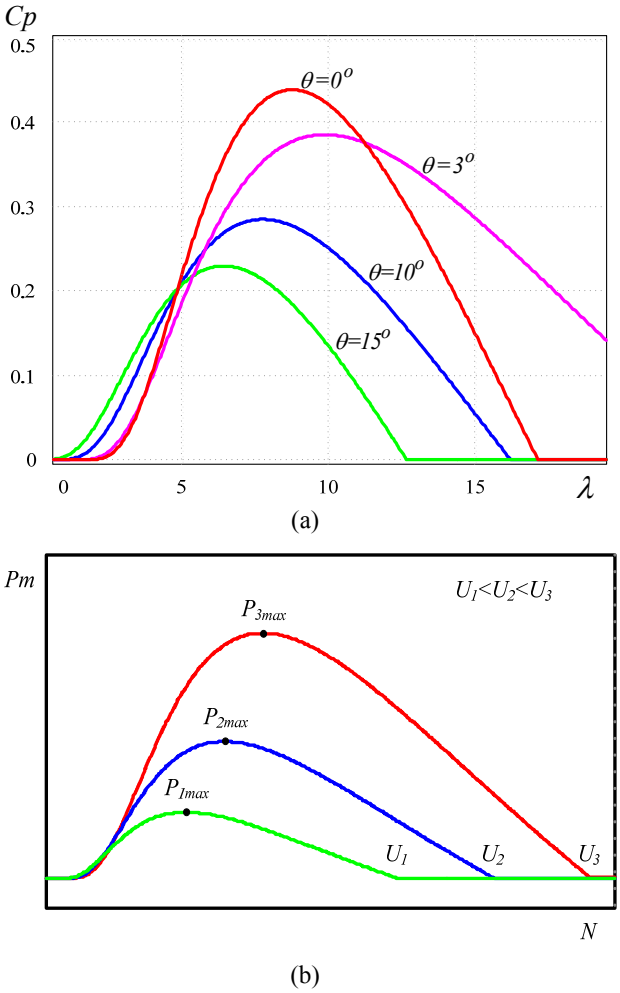

Fig. 1 Characteristic curves of (a) Cp-λ for different blade pitch angles and (b) Pm-N under different wind speeds.

For safety reasons, currently, most of the rated operating points of commercially available small WTGs are set to the power value corresponding to a 12 m/s wind speed. Therefore, the related experimental tests carried out in this paper also adopt 12 m/s wind speed as the rated operating point, but considering the actual operation of the driver used, the wind speed of 11 m/s is selected as the maximum power operating point. The system specifications of the WTE designed in this paper are as follows: P_m = 1 kW, N = 2000 rpm, rated torque = 4.782 N-m, armature current = 5.16 A, line-to-line voltage = 185.3 V_{rms}, number of poles = 8, rotor inertia = 6.26 kg-cm^2, stator resistance = 1.82 Ω, stator inductive reactance = 10.05 mH, mechanical time constant = 1.11 ms, and torque constant = 1.017 N-m/A. The radius and pitch angle of the blades can be designed after obtaining rated power, rotational speed, and torque; it is necessary to match the parameter values reasonably. The WT model can be built using a characteristic equation close to the characteristics of an actual WT. This method is quite simple and does not require the measurement of the characteristics of a WT. P_m can then be calculated with N, U, R, θ and air density ρ, as shown in Fig. 2.

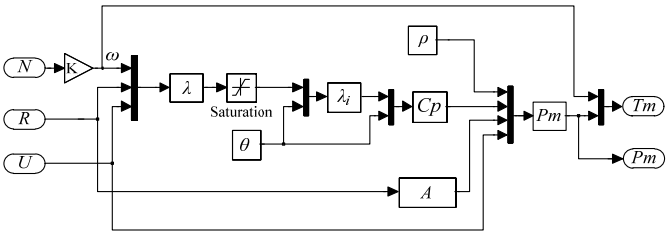

Fig. 2 The WT mathematical model

The verification task of the WT model is performed using PSIM simulating a WT with a rated capacity of 735 W, rotational speed of 1027 rpm, and torque of 6.83 N-m. The PSIM simulation model is shown in Fig. 3, with the selected parameter ρ = 1.1 kg/m^3. In the simulation, by adjusting R and θ at rated wind speed, one can finally achieve the specifications of R = 0.8 M and θ = 3°. Simulation results of *Pm*-*N* characteristics are shown in Fig. 4.

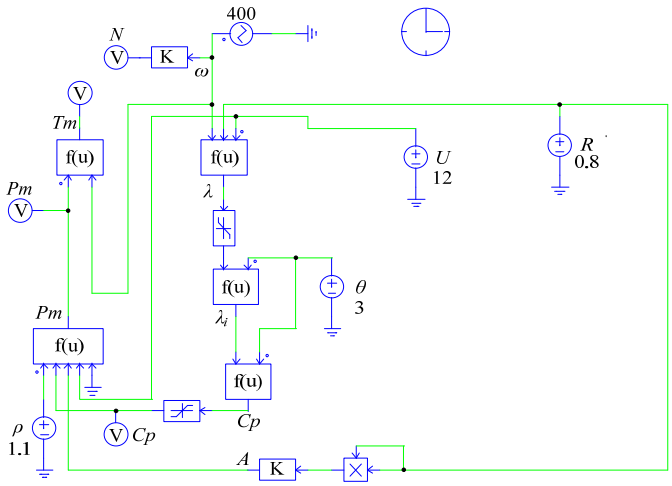

Fig. 3 PSIM simulation model of a WT.

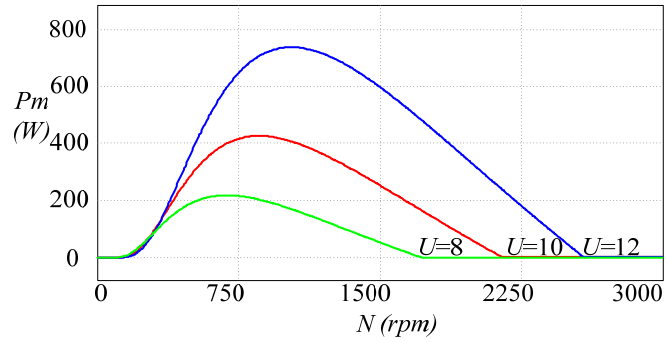

Fig. 4 PSIM simulation results of a WT characteristics.

3. PERMANENT MAGNET WIND TURBINE GENERATION SYSTEM

3.1 Mathematical Model of a Permanent Magnet Wind Turbine Generator

The rotor of a PMSG studied in this paper is a surface-mounted permanent magnet (SMPM), so its magnetic flux can be regarded as a constant. The stator is composed of a set of three-phase winding; the three windings are 120° electrical angle apart from one another, and the equivalent winding inductance N_s and resistance value r_s of each phase being identical. Fig. 5 (a) shows the three-phase Y-connection of the PMSG, which can be simplified to a single-phase equivalent circuit shown in Fig. 5 (b). The phasor diagram of the circuit in generator mode is shown in Fig. 6.

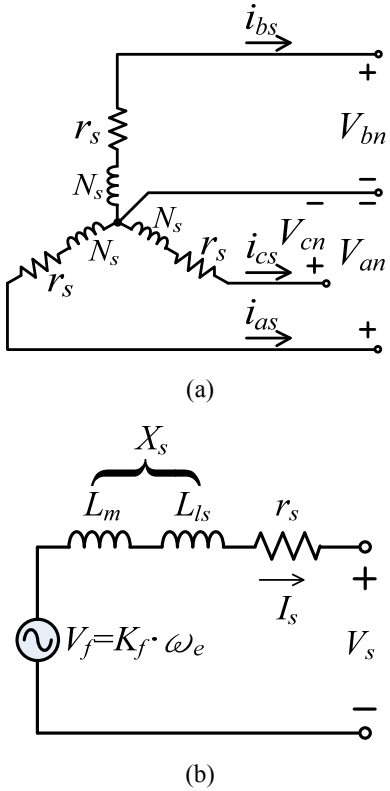

Fig. 5. Three-phase Y-connection of PMSG: (a) equivalent circuit and (b) single-phase equivalent circuit.

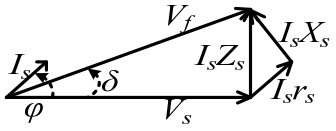

Fig. 6 Phasor diagram of the equivalent circuit in generator mode.

To independently adjust the torque and magnetic field of the PMSG, we use steady-state d-q axis voltage equations of the PSMG as follows:

$$\omega_e \lambda'_m = v_q + r_s i_q + \omega_e L_d i_d ; \tag{2}$$

$$0 = v_d + r_s i_d + \omega_e L_q i_q . \tag{3}$$

Electromagnetic torque T_e can be expressed as

$$T_e = \frac{3}{2}\frac{P}{2}\lambda'_m i_q , \tag{4}$$

and the dynamics of the mechanical system is as follows:

$$T_e = J_m \frac{d}{dt}\omega_r + B\omega_r + T_L = J_m \frac{d}{dt}\frac{2}{P}\omega_e + B\frac{2}{P}\omega_e + T_L , \tag{5}$$

where J_m represents the moment of inertia, B represents the coefficient of viscosity, T_L represents the load torque, ω_r represents generator angular velocity, and ω_e represents electromagnetic angular velocity. A simple analogy between electricity and machinery is used in this paper, shown in Fig. 7, to perform the required conversion, where I_m represents generator current, I_L represents load current, and J represents moment of inertia. The current source in the figure can be regarded as the parameter of torque. Dividing the output power by the speed yields a torque value which is regarded as a current source. Finally, a voltage signal is used to control the current source to control the power output of the WT model and achieve the coupling mechanism between electrical and mechanical energies.

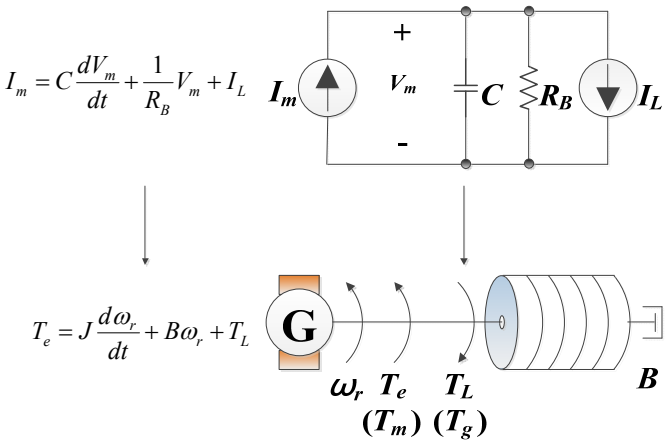

Fig. 7 Relationship between electricity and machinery systems.

Fig. 8 shows the constructed mechanical coupling model of a WT-generator in PSIM software environment, where the WTG model outputs a torque signal, which provides a power signal to the voltage-controlled current source through the control-power (C/P) interface block built in the PSIM software. Then, the voltage is output via the RC circuit, where the Zener diode is used to limit the maximum voltage. Finally, the voltage output from the RC circuit is converted into mechanical power through the electrical-mechanical (E/M) interface block module built in the PSIM software for driving the generator.

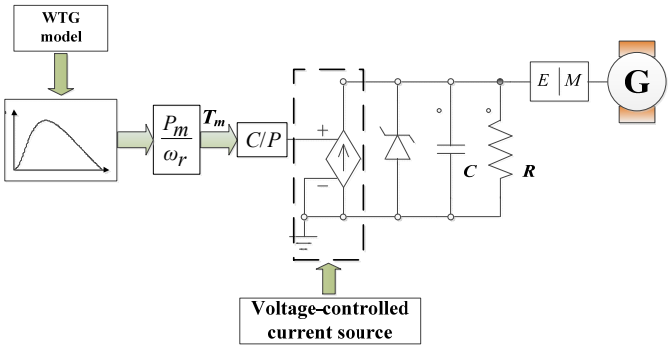

Fig. 8 The coupling model of WT and generator.

3.2 System-wide Simulation and Analysis of Permanent Magnet Wind Turbine Emulator

In order to verify the proposed mathematical models and the related design methods of WTE and generator, this paper develops a 0.7 kW WTE on a PMSG using the PSIM simulation environment, as shown in Fig. 9. In the model, a rotational speed command for maximum power known at a certain wind speed is given to control the generator. Simulation results are shown in Fig. 10, including (a) rotational speed N and its command N^*, (b) three-phase output voltages V_a, V_b, and V_c, (c) generator input mechanical power P_m and final electrical output power P_o, and (d) generator output torque T_m and coefficient of power C_p. When N is set for the maximum power point (U = 12 m/s), the WT can indeed output approximately 0.7 kW power, which verifies the correctness and accuracy of the WTE designed in section 2.

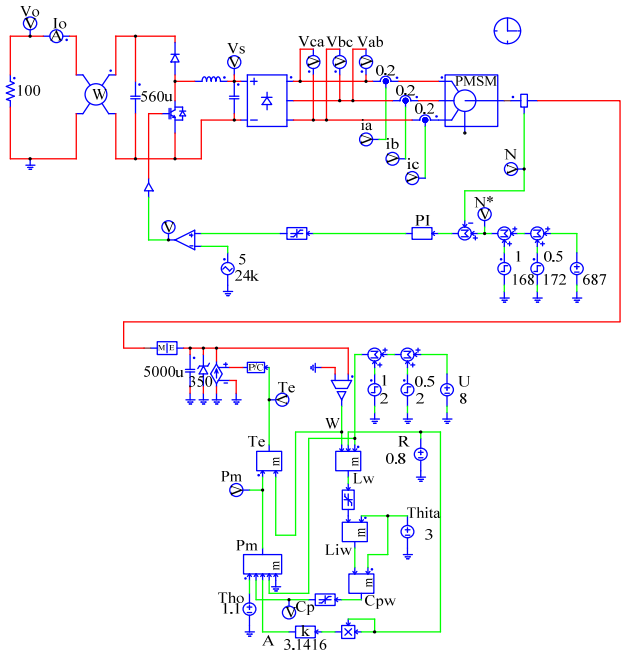

Fig. 9. Simulation of 0.7 kW WTE system.

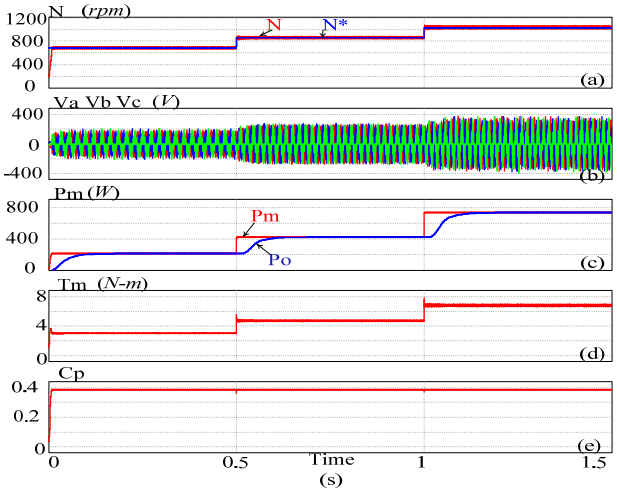

Fig. 10. Simulation results of 0.7 kW WTE system.

4. HARDWARE IMPLEMENTATION OF THE WTG EMULATOR SYSTEM

4.1 System Architecture

Figure 11 shows the architecture of the proposed hardware implementation system of a WTG, including a WTE unit, a three-phase PMSG unit, and a power converter unit. The change in wind speed will change the torque command, and then the

command is transmitted to the motor drive with the AD/DA card to drive the motor. The motor's rated specifications in this hardware emulation system are as follows: power = 1 kW, rotational speed = 2000 rpm, lint-to-line voltage = 220 V_{rms}, torque = 5 N-m, and number of pols = 8. The rated torque sensor specifications are as follows: capacity = 50 N-m, rotational speed = 5000 rpm, corresponding to a voltage output = ± 5 V.

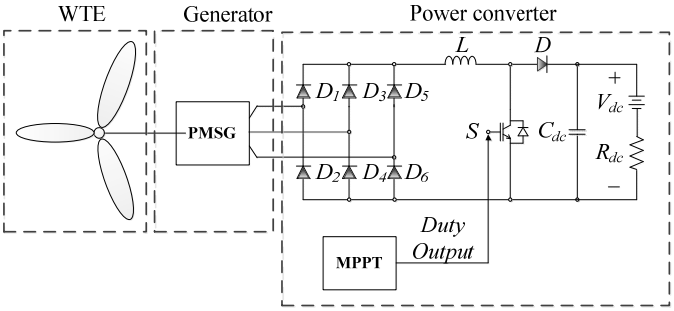

Fig. 11 System architecture of the WTG implementation.

This paper adopts direct torque control, which is a variable frequency speed control technology that has grown more popular after the development of field-oriented control. The basic control principle is to estimate the stator flux and electromagnetic torque using stator current and voltage, then subtract them with their respective commands to obtain the error values, and finally drive the motor through generating appropriate voltage and current vectors according to the error values. There is a number of advantages for using direct torque control, including no need for inner loop current control, no complex decoupling operations, simple control architecture, and fast torque dynamic response [20]. As can be seen in Fig. 11, the power control interface of the proposed WTG adopts a simple three-phase full-bridge rectifier and a boost DC-DC converter.

4.2 Torque Tracking Controller

Fig. 12 shows the control architecture used in the experiments carried out in this paper. As mentioned earlier, the existing motor torque driver adopts a simple proportional (P) controller. The parameter setting of the controller adopts the rule of thumb. In order to further improve the torque tracking performance, this paper uses proportional integral (PI) and fuzzy controllers to redesign the controller.

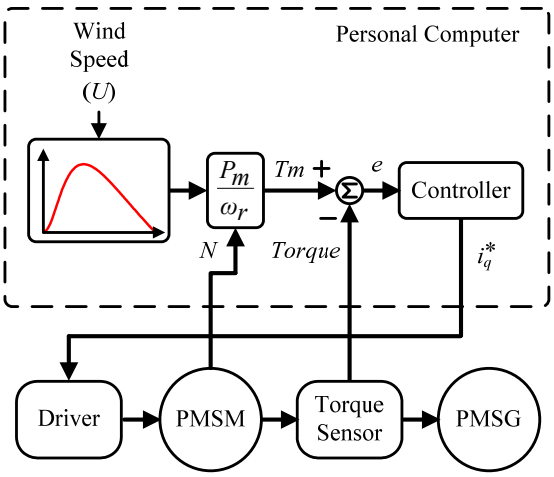

Fig. 12 Torque tracking controller and system architecture.

4.2.1 PI controller

PI controllers are known as having good stability, simple structure and easy adjustment, and are reliable in most digital control applications. Fig. 13 shows the block diagram of PI control system, where $E(s)$ represents error signal in s domain, and $U(s)$ represents output signal in s domain:

$$U(s) = k_i \frac{E(s)}{s} + k_p E(s). \tag{6}$$

Converting (6) into time domain yields

$$u(t) = k_i \int e(t)dt + k_p e(t). \tag{7}$$

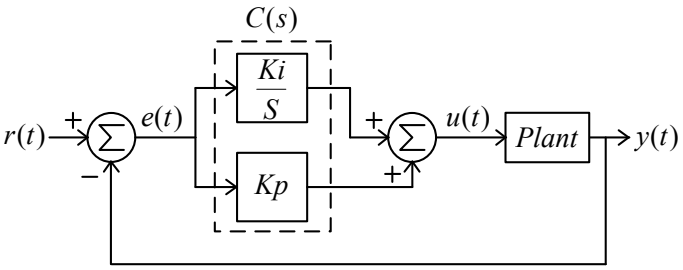

Fig. 13 PI control loop.

The proposed PI control system is shown in Fig. 14, and its close-loop transfer function is as follows:

$$T(s) = \frac{Y(s)}{R(s)} = \frac{K_p K s + K_i K}{s^2 + (K_p K + T_m)s + K_i K}. \tag{8}$$

Letting the input command a step signal and letting $R(s) = 1/s$ yield

$$E(s) = \frac{s^2 + T_m s}{s^2 + (K_p K + T_m)s + K_i K} \cdot \frac{1}{s} = \frac{s + T_m}{s^2 + (K_p K + T_m)s + K_i K}. \tag{9}$$

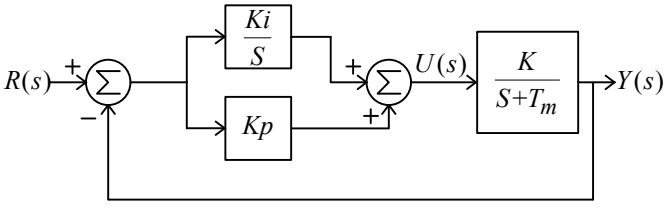

Fig. 14 Block diagram of PI motor control system.

Next, from a preliminary experimental test, motor parameters, k = 20 and T_m = 5.46 are obtained. The transfer function derived from the above equation can be obtained as follows:

$$T(s) = \frac{Y(s)}{R(s)} = \frac{20(K_p s + K_i)}{s^2 + (20K_p + 5.46)s + 20K_i}. \tag{10}$$

The control requirements of this system include maximum overshoot P.O. ≤ 1% and settling ling time $t_s \leqq 0.5$s, which yields $0.7 \leq \xi < 1$ and $t_s = 4/\xi\omega n \leq 0.5$s, and thus the following result can be obtained:

$$\frac{Y(s)}{R(s)} = \frac{\omega_n^2}{s^2 + 2\xi\omega_n s + \omega_n^2} = \frac{(11.43)^2}{s^2 + 2(0.7)(11.43)s + (11.43)^2}. \quad (11)$$

Finally, we get $k_p = 0.527$ and $k_i = 6.53$.

4.2.2 Fuzzy controller

A fuzzy controller use control rules similar to languages that human operators can understand. In order to combine the input deterministic values with the linguistic control rules, a fuzzification interface is necessary to map the inputs into the fuzzy controller language domain. A fuzzy set corresponds the inputs to the output values of its membership function (between 0 and 1), with various degrees of approximation. The design of a fuzzy controller can be divided into the following four parts. First, the fuzzification interface converts the input values into subjective values, that is, converts real numbers into a continuous membership function with fuzzy numbers. Commonly used methods include increasing S function, decreasing Z function, and Gaussian function with possible membership functions of pricewise continuous triangular function and pricewise continuous trapezoidal function. In this paper, the triangular membership function is used and 7 language variables are applied for torque error and torque error variation, including PB, PM, PS, NS, NM, NB (the first letter represents positive or negative, and the second letter represents big, medium, or small), and ZE represents zero error. Triangular membership function is less computationally intensive; if a more rigorous control performance is required, a membership function with a higher slope must be used.

Second, fuzzy control works through rules defined by the fuzzy rule base. These rules will try to make the control of the entire system according to the desired response. These rules normally decide the performance of the controller. Fig. 15 shows the scope of language variables and domain designed in this paper. After confirming the control values corresponding to the control rules and the required dynamic response, we can then construct the control rules as organized in Table 1.

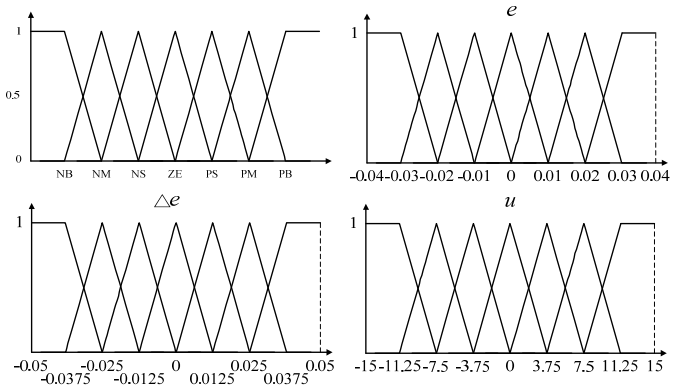

Fig. 15 The language variables and value domain designed for the fuzzy controller.

Table 1 Fuzzy control rules.

u		*e*						
		NB	NM	NS	ZE	PS	PM	PB
Δ*e*	NB	ZE	ZE	NS	NB	ZE	ZE	PS
	NM	ZE	NM	NS	NM	ZE	PS	PM
	NS	NB	NM	NS	NS	PS	PM	PB
	ZE	NB	NM	NS	ZE	PS	PM	PB
	PS	NB	NB	NS	PS	PS	PS	PB
	PM	NB	NM	NS	PM	PS	PM	PB
	PB	NM	NS	NS	PB	PM	PB	PB

Third, fuzzy inference engine is the major part of the whole fuzzy control system. Through the inference, it determines the decision-making of the system output. It is hoped that the inference can work as close to the judgment of the human being as possible. The inference mechanism is based on the control rules provided by the rule base. After the fuzzy inference, the appropriate output value is obtained for the defuzzification. The fuzzy inference calculation methods include max-min composition, product, and monotonic membership function.

Finally, the defuzzification interface converts the conclusions produced by the fuzzy inference into specific output values. The commonly used defuzzification method is center of area method, which has the advantage of being simple and easy to use, but it can result in too much calculation due to the irregularity of the membership function. The formula of center of area is as follows:

$$u^* = \frac{\int x \cdot U(x)dx}{\int U(x)dx}. \quad (12)$$

4.3 Basic Testing and Measurement

Fig. 16 shows the block diagram of the hardware implementation for performing basic tests. In this test, the wind speed is set to a fixed value, and the autotransformer is randomly adjusted to change the output power. A number of measured data under the given wind speed are recorded and compared with previously recorded data of an actual generator for the verification of correctness. The test results with fixed wind speeds of 6 m/s and 10 m/s are shown in Fig. 17 (a) and (b), respectively, where P_m-$N(s)$ represents simulated P_m-N characteristics, and P_m-$N(c)$ represents the implemented P_m-N characteristics. From the results, it can be found that, with a given fixed wind speed, the adjustment of the output voltage affects the WTE power, and the recorded power curve is in good agreement with the simulated power curve. The load power curve recorded has some power loss due to the autotransformer and the circuit.

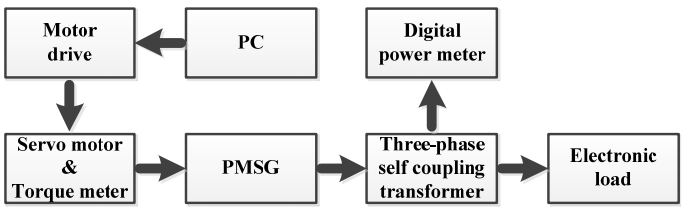

Fig. 16 Hardware architecture for performing basic tests.

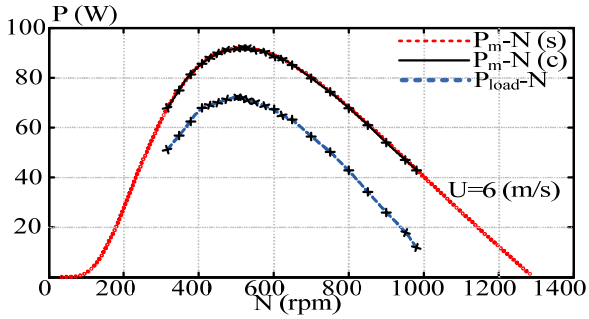

(a)

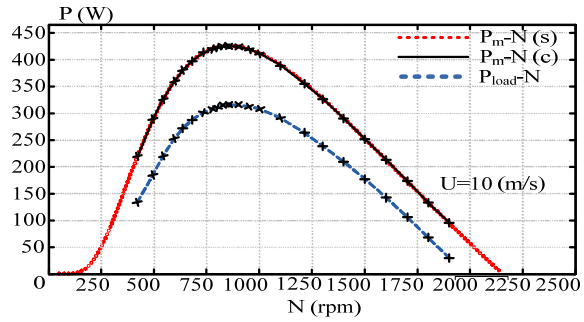

(b)

Fig. 17 Basic test of WTE system with fixed wind speed: (a) wind speed = 6 m/s (Pm-N(s)max = 91.91 W @ N = 515.7 rpm, Pm-N(c)max = 91.83 W @ N = 512.7 rpm, and Pload-Nmax = 72 W @ N = 510 rpm); (b) wind speed = 10 m/s (Pm-N(s)max = 425.8 W @ N = 859.5 rpm, Pm-N(c)max = 425.5 W @ N = 860 rpm, and Pload-Nmax = 316 W @ N = 860 rpm)

4.4 Complete System Implementation

The complete hardware implementation of the WTG emulator is conceptually shown in Fig. 18. The experimental specifications are as follows: wind speed U = 4-12 m/s, air density ρ = 1.1 kg/m^3, blade radius R = 0.8 m, blade pitch angle θ = 3°, rated power P = 735 kW, rated rotational speed N = 1027 rpm, and rated torque T = 8.28 N-m. Twenty wind speeds are assigned within 3-11 m/s.

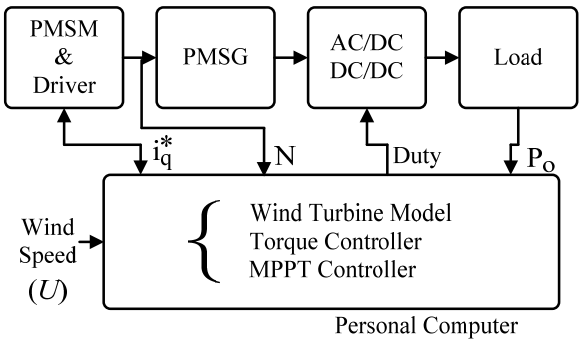

Fig. 18 The complete hardware implementation of the proposed WTG emulator.

4.4.1 Torque Tracking Control Test and Results

In the tests of various torque tracking control methods, the wind speed varies with step changes every 0.5s, with a total of 20 changes. Fig. 19 shows the wind speed command U, generator torque and its command T_g & T_m, torque error, and integral of squared-error (ISE) of torque tracking control based on (a) P controller, (b) PI controller, and (c) fuzzy controller. Figure 20 compares the ISE of the three control methods.

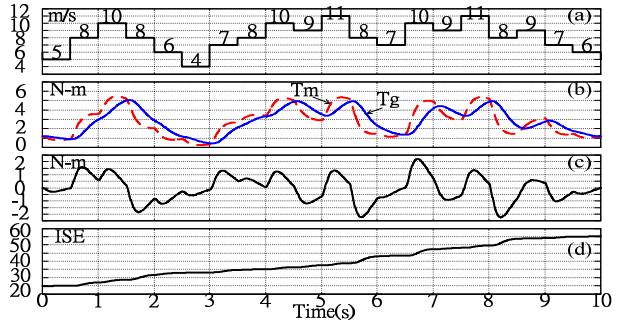

(a)

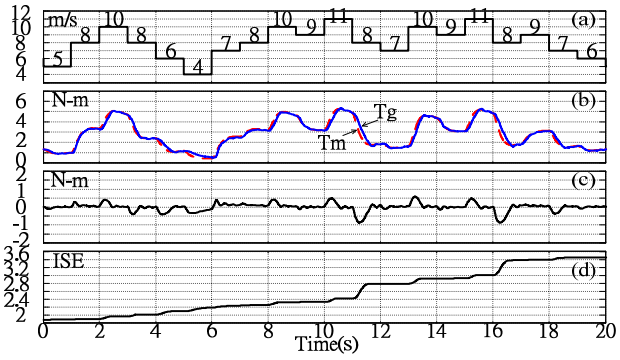

(b)

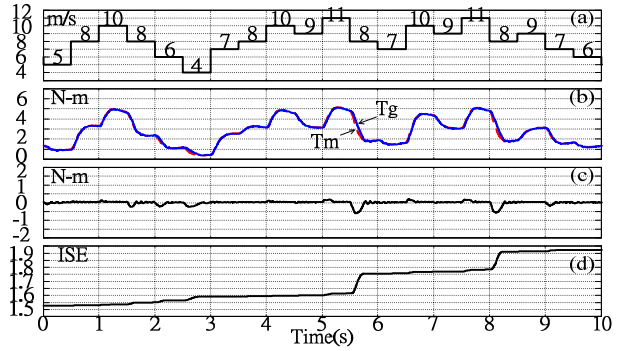

(c)

Fig. 19 Results of the test of various torque tracking controllers: (a) P controller, (b) PI controller, and (c) Fuzzy controller.

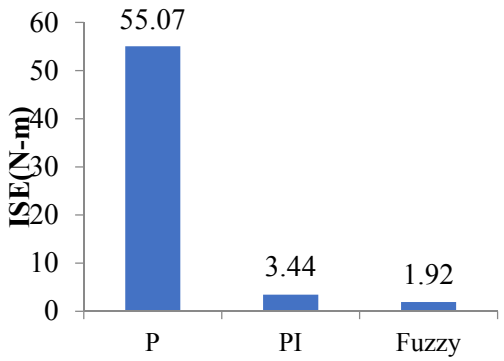

Fig. 20 The ISE comparison among the three controllers.

4.4.2 System Functional Test and Results

Fig. 21 shows a set of P_m-N characteristics at different wind speeds. In this test, the perturb-and-observe algorithm is used as wind speed varies in step changes every 20s, with a total of 6 changes. Figs. 22 (a) & (b) show the simulation and experimental test results, respectively, including wind speed command U, generator torque T_e, generator power output P_m, generator rotational speed N, and coefficient of power C_p. Fig. 23 shows load voltage, current and power (V_{load}: 50 V/div, I_{load}: 2.5 A/div, P_{load}: 200 W/div). It can be seen from the recorded waveforms that the implementation results are very similar to the simulation results, which verifies the correctness of the proposed torque tracking algorithm.

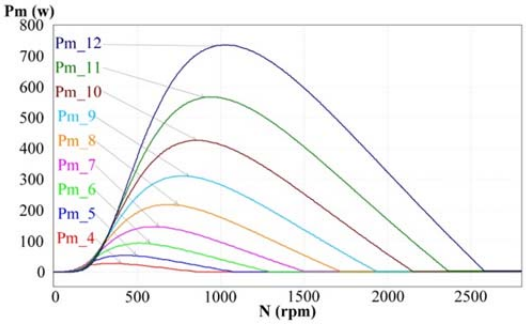

Fig. 21 WT Pm-N characteristics at different wind speeds.

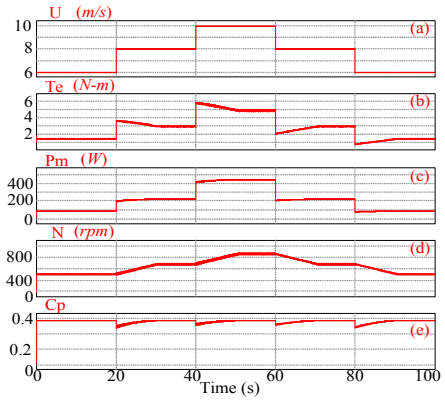

(a)

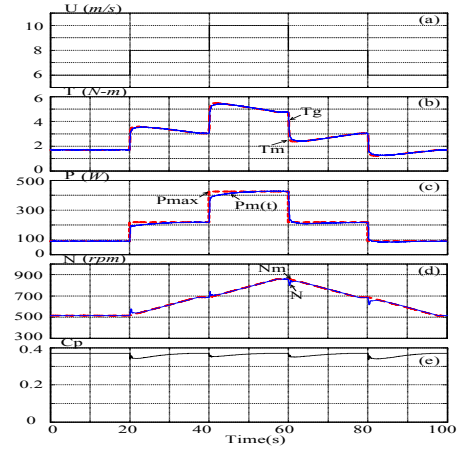

(b)

Fig. 22 Results of perturb and observe method with step changes in wind speed: (a) simulation results and (b) implementation results.

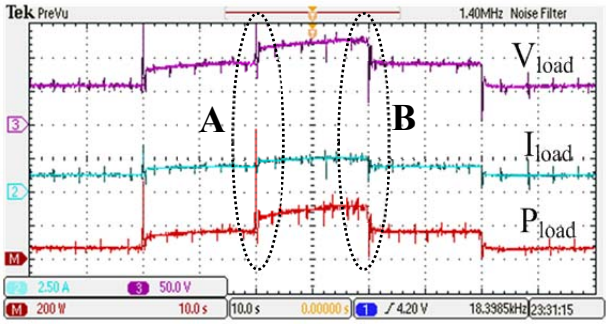

(a)

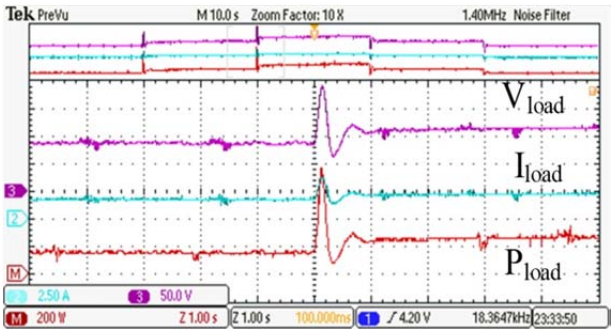

(b)

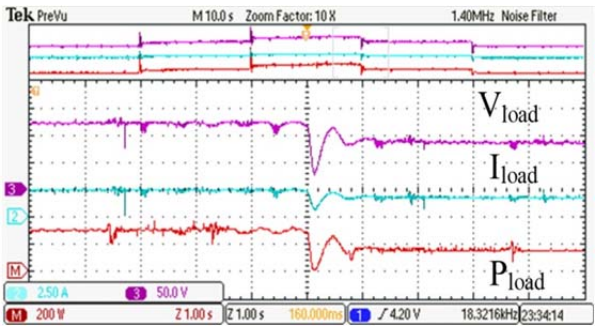

(c)

Fig. 23 The measured waveforms of load voltage, current and power: (a) overall view, (b) detailed view at switching point A, and (c) detailed view at switching point B.

5. CONCLUSION

This paper has presented a design example of a small permanent magnet synchronous WTE system. With the proposed design method, the parameters of the WT can be changed at any time depending on the needs in emulating various WT characteristics. The proposed WTE system can provide researchers with a high flexibility and a more convenient test environment in conducting various WECS research. In this paper, WT and PMSG models have been successfully integrated and the technique of real-time control has been used to facilitate the necessary parameters acquisition and implementation of digital controllers. The operation of a complete WTG system has been accurately emulated with experimental hardware system and the proposed controllers. Typical test results obtained from the proposed WTG emulator are in good consistent with the theoretical data, verifying the feasibility and correctness of the proposed design method.

ACKNOWLEDGEMENTS

The authors would like to thank the Ministry of Science and Technology (MOST) of Taiwan for financially support this study regarding renewable energy power generation and energy conversion and storage related researches. Grant numbers: MOST Taiwan: MOST. 110-2221-E-239-032.

REFERENCES

Abdallah, M. E., Arafa, O. M., Shaltot, A., & Aziz, G. A. A. (2018). "Wind turbine emulation using permanent magnet synchronous motor." *Journal of Electrical Systems and Information Technology*, **5**(2), 121-134.

Ackermann, T. (2005). *Wind power in power systems* (Vol. 200, No. 5). New York: Wiley.

Ajewole, T. O., Alawode, K. O., Omoigui, M. O., & Oyekanmi, W. A. (2017). "Design validation of a laboratory-scale wind turbine emulator." *Cogent Engineering*, **4**(1), 1280888.

Arévalo, F., Estrada, P., Pozo, N., & Pozo, M. (2017, October). "Wind generation emulator using a DC machine." In *2017 IEEE Second Ecuador Technical Chapters Meeting (ETCM)* (pp. 1-6). IEEE.

Bhayo, M. A., Aziz, M. J. A., Idris, N. R. N., & Yatim, A. H. M. (2017). "Design and development of a wind turbine emulator for analyzing the performance of stand-alone wind energy conversion system." *International Journal of Power Electronics and Drive Systems (IJPEDS)*, **8**(1), 454-461.

Bhukya, J., & Mahajan, V. (2018, December). "Modelling of Power System Stabilizer for Double Fed Induction Generator based Wind Power System." In *2018 IEEE 8th Power India International Conference (PIICON)* (pp. 1-6). IEEE.

Chen, P. Y., Hu, K. W., Lin, Y. G., & Liaw, C. M. (2017). "Development of a prime mover emulator using a permanent-magnet synchronous motor drive." *IEEE Transactions on Power Electronics*, **33**(7), 6114-6125.

Chen, Q., Li, W., & Chen, G. (2016). "FUZZY P+ ID controller for a constant tension winch in a cable laying system." *IEEE Transactions on Industrial Electronics*, **64**(4), 2924-2932.

Gan, L. K., Shek, J. K., & Mueller, M. A. (2017). "Modeling and characterization of downwind tower shadow effects using a wind turbine emulator." *IEEE Transactions on Industrial Electronics*, **64**(9), 7087-7097.

Guerrero, J. M., Lumbreras, C., Reigosa, D. D., Garcia, P., & Briz, F. (2017). "Control and emulation of small wind turbines using torque estimators." *IEEE Transactions on industry applications*, **53**(5), 4863-4876.

Karabacak, M., Küçük, T. V., Atmaca, Ö., Kamal, T., & Cantaş, Y. (2018). "Design and Implementation of a Wind Turbine Emulator for Wind Energy Conversion Systems." In *7th International Conference on Advanced Technologies* (pp. 135-139).

Liu, K., Hou, C., & Hua, W. (2019). "A novel inertia identification method and its application in PI controllers of PMSM drives." *IEEE Access*, *7*, 13445-13454.

Merabet, A., Ahmed, K. T., Ibrahim, H., Beguenane, R., & Ghias, A. M. (2016). "Energy management and control system for laboratory scale microgrid based wind-PV-battery." *IEEE transactions on sustainable energy*, **8**(1), 145-154.

Mohammadi, E., Fadaeinedjad, R., & Naji, H. R. (2018). "Using a new wind turbine emulator to analyze tower shadow and yaw error effects." *Energy Conversion and Management*, *174*, 378-387.

Mohammadi, E., Fadaeinedjad, R., Naji, H. R., & Moschopoulos, G. (2018). "Investigation of horizontal and vertical wind shear effects using a wind turbine emulator." *IEEE Transactions on Sustainable Energy*, **10**(3), 1206-1216.

Narayana, M., Sunderland, K. M., Putrus, G., & Conlon, M. F. (2017). "Adaptive linear prediction for optimal control of wind turbines." *Renewable Energy*, *113*, 895-906.

Qais, M. H., Hasanien, H. M., & Alghuwainem, S. (2017). "Low voltage ride-through capability enhancement of grid-connected permanent magnet synchronous generator driven directly by variable speed wind turbine: a review." *The Journal of Engineering*, **2017**(13), 1750-1754.

Sampaio, L. P., da Rocha, M. V., da Silva, S. A. O., & de Freitas, M. H. T. (2019). "Comparative analysis of MPPT algorithms bio-inspired by grey wolves employing a feed-forward control loop in a three-phase grid-connected photovoltaic system." *IET Renewable Power Generation*, **13**(8), 1379-1390.

Shukla, S., & Singh, B. (2019). "Adaptive speed estimation with fuzzy logic control for PV-grid interactive induction motor drive-based water pumping." *IET Power Electronics*, **12**(6), 1554-1562.

Tian, J., Liu, J., Shu, J., Tang, J., & Yang, J. (2018). "Engineering modelling of wind turbine applied in real-time simulation with hardware-in-loop and optimising control." *IET Power Electronics*, **11**(15), 2490-2498.

Xia, C., Li, S., Shi, Y., Zhang, X., Sun, Z., & Yin, W. (2019). "A non-smooth composite control approach for direct torque control of permanent magnet synchronous machines." *IEEE Access*, *7*, 45313-45321.